JOURNAL OF THE ROYAL SOCIETY Interface

rsif.royalsocietypublishing.org

Research

Cite this article: Ventre M, Natale CF, Rianna C, Netti PA. 2014 Topographic cell instructive patterns to control cell adhesion, polarization and migration. *J. R. Soc. Interface* **11**: 20140687.
http://dx.doi.org/10.1098/rsif.2014.0687

Received: 27 June 2014
Accepted: 4 September 2014

Subject Areas:
biomaterials, bioengineering

Keywords:
topographic patterns, cell adhesion, cell migration, focal adhesions

Author for correspondence:
Paolo Antonio Netti
e-mail: nettipa@unina.it

Electronic supplementary material is available at http://dx.doi.org/10.1098/rsif.2014.0687 or via http://rsif.royalsocietypublishing.org.

Royal Society Publishing

Topographic cell instructive patterns to control cell adhesion, polarization and migration

Maurizio Ventre[1,2,3], Carlo Fortunato Natale[3], Carmela Rianna[1,2,3] and Paolo Antonio Netti[1,2]

[1]Department of Chemical, Materials and Industrial Production Engineering, and [2]Interdisciplinary Research Center on Biomaterials, University of Naples Federico II, Piazzale Tecchio 80, 80125 Naples, Italy
[3]Center for Advanced Biomaterials for Health Care@CRIB, Istituto Italiano di Tecnologia, Largo Barsanti e Matteucci 53, 80125 Naples, Italy

Topographic patterns are known to affect cellular processes such as adhesion, migration and differentiation. However, the optimal way to deliver topographic signals to provide cells with precise instructions has not been defined yet. In this work, we hypothesize that topographic patterns may be able to control the sensing and adhesion machinery of cells when their interval features are tuned on the characteristic lengths of filopodial probing and focal adhesions (FAs). Features separated by distance beyond the length of filopodia cannot be readily perceived; therefore, the formation of new adhesions is discouraged. If, however, topographic features are separated by a distance within the reach of filopodia extension, cells can establish contact between adjacent topographic islands. In the latter case, cell adhesion and polarization rely upon the growth of FAs occurring on a specific length scale that depends on the chemical properties of the surface. Topographic patterns and chemical properties may interfere with the growth of FAs, thus making adhesions unstable. To test this hypothesis, we fabricated different micropatterned surfaces displaying feature dimensions and adhesive properties able to interfere with the filopodial sensing and the adhesion maturation, selectively. Our data demonstrate that it is possible to exert a potent control on cell adhesion, elongation and migration by tuning topographic features' dimensions and surface chemistry.

1. Introduction

Biological tissues display a vast variety of topographies such as fibrils, fibre bundles, pits and protrusions, whose characteristic dimensions span from tens of nanometres up to the micrometre scale [1–3]. It is therefore reasonable to expect that the presentation of topographic signals is one of the strategies that Nature adopts to impart to cells specific orders, which eventually dictate their behaviour. In fact, many works demonstrated that patterned substrates strongly influence cell adhesion, migration and differentiation, suggesting that the presentation of topographic signals might be a powerful tool to control and guide cell behaviour *in vitro* [4–8]. Indeed, recent literature has addressed the importance of the material–cytoskeleton crosstalk, which is at the helm of the biophysical and biochemical stimuli eventually governing cell fate and functions [9]. These studies show novel routes to design bioinspired surfaces for biotechnological applications: several techniques proved to be adequate to produce micro- and nano-patterns with high precision and long range-order [10,11]. Yet, the implementation of such technologies for the production of patterned biomedical devices is still in its infancy. This limitation is mainly caused by our incomplete knowledge of how cells perceive and react to topographic signals. Furthermore, cell responses vary enormously according to topographic features and dimensions, making it difficult to identify those characteristic dimensions which may be relevant for biomedical applications.

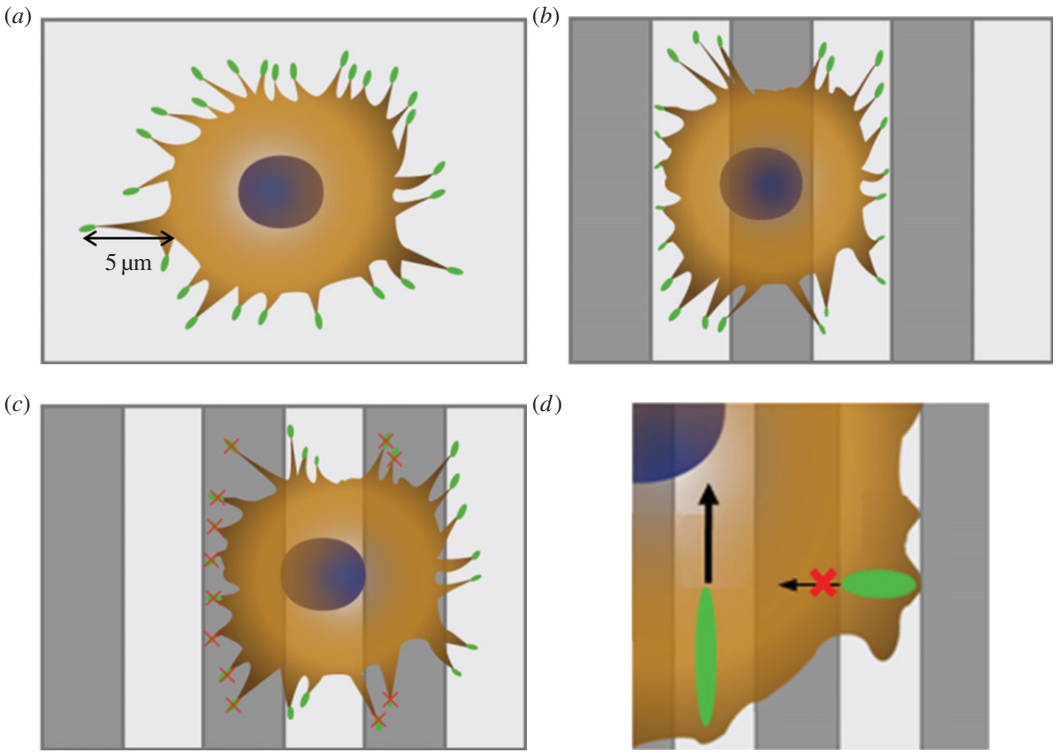

Figure 1. Schematic of the micrometre scale topography sensing and cell elongation and alignment. Early mechanisms involve filopodia probing. We assumed a characteristic length of the filopodium of 5 μm (*a*). If the distance is larger, filopodia cannot bridge several ridges (*b*) and the cell body polarizes only on a limited number of them (*c*). On narrower topographic features (2 μm), FAs can grow considerably and their length surpasses the ridge dimension (*d*). In this case, FA growth occurs predominantly along the pattern and the cell body polarizes consequently. (Online version in colour.)

In an *in vivo* context, it is desirable to control specific cell processes such as migration, proliferation and tissue biosynthesis. Despite the large numbers of works that have been developed so far on cell–topography interactions, a general consensus on what settings of topographic features elicit specific cell functions has not been reached yet. For example, while certain combinations of topographies promote cell alignment and migration, others report different trends [12,13].

This raises the fundamental question on how cells perceive and react to topographies. In this study, we chose to address this issue by using microtopographic patterns whose features might interfere with the cellular mechanisms that lead to material surface sensing. Among these processes, many studies pointed out that filopodial probing and cell adhesion formations are crucial for the recognition of and the reaction to material surface characteristics. Filopodia are thin and few micrometre long protrusive processes constituted by parallel bundles of filamentous actin [14]. Their tips display molecular receptors like integrins and cadherins, making filopodia the tactile sensors for the establishment of contacts in the extracellular space. Although filopodia length may vary considerably among cells, it has been reported that it falls within the micrometre scale range. In particular, the characteristic length of a filopodium projecting out of the cell membrane is approximately 5 μm [15]. Therefore, topographic features of the surface or protrusions 5 μm beyond the cell membrane might not be readily sensed by filopodia. Once filopodia have attached to the surface, they constitute the template for cell membrane extension and eventually adhesion formation.

Cell adhesions are dynamic molecular complexes for which formation, maturation and disassembly phases can be distinguished [16]. Nascent adhesions initiate with the binding of transmembrane receptors—integrins—to extracellular ligands. These complexes can grow only if firmly anchored to the surface, in which case additional intracellular proteins are recruited to the adhesion site, creating macromolecular complexes referred to as focal adhesions (FAs). Usually, adhesions are classified as focal if their length is between 1 and 5 μm [17]. These large variations in FA lengths mainly depend on the surface chemistry and ligand availability and density. In particular, surface hydrophilicity alters the presentation of ligands on the surface and any changes in material wettability have a profound effect on FA formation and growth [18]. Therefore, by simply altering hydrophobicity or hydrophilicity of the surface, for example by performing surface treatments, FA maturation can be depressed or promoted, respectively. Furthermore, surface topography may regulate the geometrical features of maturing FAs by displaying zones that are conducive for integrin clustering (e.g. ridges), juxtaposed to others that do not permit the formation of integrin–ligand complexes (like deep recesses or grooves). Therefore, FA shape and spatial arrangement can be in principle tuned through specifically designed topographic patterns.

In order to limit FA formation on the protrusions thus making the recesses less accessible, we set the feature depth at 1 μm, recently reported as the characteristic depth that discourages FA formations on the pits of polydimethylsiloxane (PDMS) microgrids [19]. In this work, we investigated the role played by cell environmental sensing, filopodial probing or adhesion establishment and growth in the perception of and reaction to surface topography. To this end, two different topographic patterns, in the form of parallel gratings, were produced in order to interfere selectively with the filopodial probing of FA growth. In particular, we hypothesize that topographic pattern recognition and subsequent reaction is a two-step process: firstly, filopodia length defines the breadth of the area in which adhesions can be formed (figure 1*a*)—if the surface features most favourable for FA formation (pattern ridges) are farther apart than the filopodia length (figure 1*b*),

cells remain confined on a specific pattern area and hence polarize (figure 1*c*); secondly, if FA growth is hindered by topographic features (ridge width), then FAs have a preferential direction of growth and maturation (figure 1*d*), which eventually dictates cell elongation.

2. Material and methods

2.1. Preparation and characterization of micropatterned substrates

Patterned substrates were obtained by replica moulding of PDMS (Sylgard 184, Dow Corning Corporation, Midland, MI, USA) on silicon masters provided by Scriba Nanotecnologie (Bologna, Italy). The masters consisted of parallel and straight ridges of photoresist channels. Two types of masters were used: one with 2 μm wide ridges and 2 μm wide grooves, the other with 5.5 μm wide ridges and 4 μm wide grooves. Both of them had 1 μm deep grooves. PDMS was prepared by mixing elastomer base and curing agent at 10 : 1 weight ratio. The solution was degassed, poured onto the Si master and then cured at 37°C for 24 h. Control (flat) PDMS substrates were produced by pouring the base and curing mix on a 35 mm polystyrene Petri dish (Corning, Corning, NY, USA) and curing at 37°C for 24 h. In the following, substrates will be referred to as 2 or 5 μm patterns. PDMS replicas were characterized with an atomic force microscope (NanoWizard, JPK Instruments, Berlin, Germany). Images were acquired in contact mode using a silicon nitride tip with a nominal spring constant of 0.1 N m^{-1} (MSCT, Bruker, Billerica, MA, USA). Scanning area was set at 50 × 50 μm, and images were recorded at line-scan rate of 1 Hz in air at room temperature. At least three independent imaging scans were obtained for each sample.

For cell culture experiments, PDMS samples were either treated with oxygen plasma or left untreated. Plasma treatment was performed with a Plasma Femto (Diener, Böblingen, Germany) equipped with a 13.56 MHz 100 W generator for the plasma excitation. Plasma exposure was 1 min and then substrates were sterilized by UV exposure for 15 min.

Untreated substrates were sterilized in an autoclave. Oxygen plasma-treated (PT) and untreated (noPT) substrates were incubated with serum supplemented culture medium (10%) overnight prior to cell culturing experiment.

Contact angle (CA) measurements were performed to analyse wettability of PT and noPT PDMS with an Attension Theta optical tensiometer (Biolin Scientific, Stockholm, Sweden). An amount of 4 μl of MilliQ water was dropped on substrates with 5.5 μl s^{-1} dispense rate. For every drop, five images were recorded and analysed with Young–Laplace fitting method.

2.2. Cell culture

MC3T3-E1 preosteoblasts (American Type Culture Collection, Manassas, VA, USA) were cultured in αMEM with deoxyribonucleosides, ribonucleosides and 2 mM L-glutamine (Gibco Life Technologies, Grand Island, NY, USA), supplemented with 10% fetal bovine serum (Gibco), penicillin (100 units ml^{-1}) and streptomycin (100 μg ml^{-1}). The cells were incubated at 37°C in a humidified atmosphere of 95% air and 5% CO_2, and the culture medium was changed every 2 days. After 3 days of culture, cells were detached with trypsin/EDTA (0.25% w/v trypsin/0.02 mM EDTA) (Gibco) and seeded on micro grooved or flat substrates at 2×10^3 cells cm^{-2} density.

2.3. Spreading area

Actin bundles of cells cultured on noPT and PT substrates were stained with TRITC conjugated phalloidin (Sigma, St Louis, MO, USA) at specified time points. In particular, cell cultures were fixed at 5, 30, 60, 90, 120 min and 24 h after seeding. Cell fixation was performed with 4% paraformaldehyde for 20 min and then permeabilized with 0.1% Triton X-100 (Sigma) in phosphate-buffered saline (PBS) 1×. Actin staining was performed by incubating samples with TRITC-phalloidin (Sigma) in PBS for 30 min at room temperature. Images of fluorescent cells were collected with a fluorescence inverted microscope (IX81, Olympus, Tokyo, Japan) equipped with an ORCA 2.8 digital camera (Hamamatsu Photonics, Shizuoka, Japan). Cell area was evaluated with the command Analyze Particles of Fiji. At least 15 cells were collected and analysed for each time point and each substrate.

2.4. Immunofluorescence and morphometric analysis

Immunofluorescence staining was carried out as follows. Cells were fixed and permeabilized as described above at 4 and 24 h after seeding on noPT and PT substrates. Samples were blocked in PBS/bovine serum albumin 1% solution (Sigma) for 30 min, to avoid non-specific binding.

FAs were recognized by incubating samples with anti-vinculin monoclonal antibody (clone 7F9, dilution 1 : 200; EMD Millipore, Darmstadt, Germany) for 2 h at 20°C. After incubation, substrates were washed three times with PBS (3 min per wash) and incubated with Alexa Fluor 488 conjugated goat anti-mouse antibody (dilution 1 : 1000; Molecular Probes, Life Technologies, Grand Island, NY, USA) for 30 min at 20°C. Actin staining was performed as described above. Samples were thoroughly rinsed in PBS and mounted on glass slides. Fluorescent images of FAs and actin bundles were collected with a Leica TCS SP5 confocal microscope (Leica Microsystems, Wetzlar, Germany). Samples were excited with 488 nm (vinculin) and 543 nm (actin) laser lines, and the emissions were collected in the 500–530 nm and 560–650 nm ranges, respectively.

Cell elongation was assessed from TRITC-phalloidin stained cells that were analysed with the MomentMacroJ v. 1.3 script (hopkinsmedicine.org/fae/mmacro.htm) run in Fiji. Briefly, the macro calculates the second moment of area of grey scale images. For our purposes, we evaluated the principal moments of inertia (i.e. maximum and minimum) and we defined a cell elongation index as the ratio of the principal moments (maximum/minimum). Cell orientation was defined as the angle that the principal axis of inertia formed with a reference axis, i.e. the pattern direction in the case of microgrooved substrates or the horizontal axis for flat surfaces. Electronic supplementary material, figure S1, shows representative cell elongation index values of two cells with different morphology, along with the angle of cell orientation.

Morphometric analysis (length versus orientation) of FAs was performed as follows. Digital images of FAs were firstly processed using blur command by following a modified version of the procedure proposed by Maruoka *et al*. [20]. Blurred image were subtracted from the original images using the image calculator command. The images were further processed with threshold command to obtain binarized images. Pixel noise was erased using the erode command and then particle analysis was performed in order to extract the morphometric descriptors. Only FAs whose area was above 0.5 μm^2 were included in the statistical analysis. Filopodia length was measured with the command 'measure' of ImageJ software. Only those filopodia not displaying visible vinculin spots were measured.

Statistical significance of the data was assessed by means of ANOVA test and Tukey's test for cell elongation and directional index and by a non-parametric Kruskal–Wallis test for cell orientation. Tests were run in Matlab (The MathWorks, Natick, MA, USA)

2.5. Scanning electron microscopy

Four hours after seeding, cells were rinsed with PBS and fixed in glutaraldehyde 2% (Sigma) for 2 h at room temperature. Then cells were dehydrated with ethanol series up to 100% at room temperature. Then samples were fully covered with ethanol 100% and they were critical point dried using an EM CPD 300

(Leica). The substrates were then mounted to microscope stub and sputter coated with gold (Sputter Coater 208 HR, Cressington, Watford, UK). Images were acquired with a Zeiss Ultra Plus FESEM scanning electron microscope (Oberkochen, Germany) with an accelerating voltage of 6 kV.

2.6. Time-lapse experiments

Cell migration experiments started 6 h after cell seeding on the substrates. Briefly, preosteoblasts were cultured on PT or noPT substrates. Afterwards, at least six representative regions per substrate were acquired in bright field each 10 min for 18 h. Time-lapse videos were analysed with MetaMorph (v. 6.1, Molecular Devices, Sunnyvale, CA, USA) in order to extract cell trajectories. Windrose plots of each experiment were plotted.

Directionality was assessed by evaluating the total movement of each cell along and across pattern direction as described by Biela *et al*. [21]. Briefly, let x be the pattern direction, then the directional index is defined as the ratio of the quantities defined as

$$\left.\begin{aligned} M_x &= \sum_t \sqrt{(x_{t+\Delta t} - x_t)^2} \\ \text{and} \qquad & \\ M_y &= \sum_t \sqrt{(y_{t+\Delta t} - y_t)^2}, \end{aligned}\right\} \tag{2.1}$$

where x_t and y_t are the coordinates of the cell centroid at time t and Δt is the time increment. If the directional index M_y/M_x is close to one, cells perform a perfect random walk. If $M_y/M_x < 1$, cells migrate preferentially along pattern direction.

3. Results

3.1. Substrate characterization

The experimental set-up was designed in order to provide cells with bioadhesive signals, modulated by the hydrophobicity/hydrophilicity of the surface, superimposed on a microtopographic pattern. Surface topography of PDMS replica is shown in the electronic supplementary material, figure S2. Firstly, we assessed the influence of topography and oxygen plasma treatment on surface wettability. Untreated substrates were hydrophobic, displaying CA $> 100^\circ$ (figure 2*a*). In particular, patterned substrates were more hydrophobic than flat surfaces, possibly owing to the establishment of the Cassie–Baxter wetting state [22]. Oxygen plasma treatment dramatically reduced the CA on all surfaces, with the 5 µm pattern exhibiting higher CA values (figure 2*a*). Cells, however, are cultivated in protein-rich media and surface protein adsorption might alter substrate hydrophobicity/hydrophilicity. Therefore, to unravel the combined effect of protein adsorption, oxygen plasma and topography on surface wettability, we performed CA measurements on samples preincubated with serum supplemented media. On noPT surfaces, we observed a general decrease of CA values with respect to the non-preincubated case, whereas PT substrates maintained their hydrophilic characteristics (figure 2*b* and electronic supplementary material, figure S3). These data suggested that even though protein adsorption was sufficient to make the PDMS hydrophilic, oxygen PT surfaces always showed significantly lower CA values and therefore it is expected that these two surface types might affect very differently cell behaviour in terms of spreading, adhesion and migration.

3.2. Cell spreading and cytoskeleton assembly

The effects of wettability and topography have been widely investigated individually; however, the combined influence on cell behaviour is poorly understood. To gain a better insight of such an influence on cell spreading, we measured projected area of actin stained cells at different time points up to 24 h. On both treated and untreated surfaces, cells attained a limiting spreading area within 90 min after seeding, whose value depended on the topographic features (electronic supplementary material, figure S4). After this time interval, the cell area oscillated around the limiting value, reflecting the extension/retraction cycles that occur at longer times. On oxygen PT surfaces, however, the cell area was larger with respect to that observed for cells seeded on untreated substrates. Furthermore, we observed that, irrespective of the surface treatment, cells on flat substrates were more spread than cells on 5 µm patterns. Cells on 2 µm patterns, instead, displayed an intermediate behaviour.

Then, we investigated the influence of the bioadhesive and topographic signals on the spatial arrangement of FAs and cytoskeleton assemblies. Confocal images of TRITC-phalloidin and Alexa Fluor stained vinculin revealed marked morphological differences between cells seeded on pristine and oxygen-treated surfaces. In detail, vinculin was largely diffused in the cytoplasm of cells cultivated on untreated microtopography, especially at 4 h post seeding (figure 3*a*,*b*). More intense spots of vinculin were observed at 24 h and at the termini of actin fibres, which were assembled in the form of a fine meshwork (figure 3*d*,*e*). On flat substrates, FAs were brighter and well defined, along with the cytoskeleton that was structured with thick actin bundles. Such features were observed already at 4 h and persisted at 24 h post seeding (figure 3*c*,*f*). Conversely, on PT surfaces, intensely stained

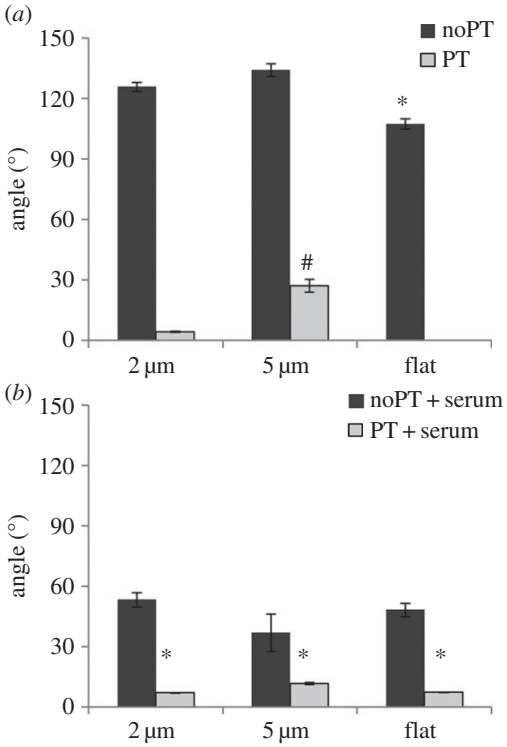

Figure 2. Histograms of the water contact angle measurements on bare patterned and flat substrates (*a*) and serum preincubated substrates (*b*). Measurements were performed both with (grey columns) or without (black columns) preliminary oxygen plasma treatment. Error bars represent the s.d. In (*a*), asterisk (*) denotes significant differences with respect to the patterned case ($p < 0.05$) and hash ($^{\#}$) represents differences with respect to the 2 µm PT case ($p < 0.05$). In (*b*), asterisk (*) denotes significant differences with respect to the noPT cases ($p < 0.05$).

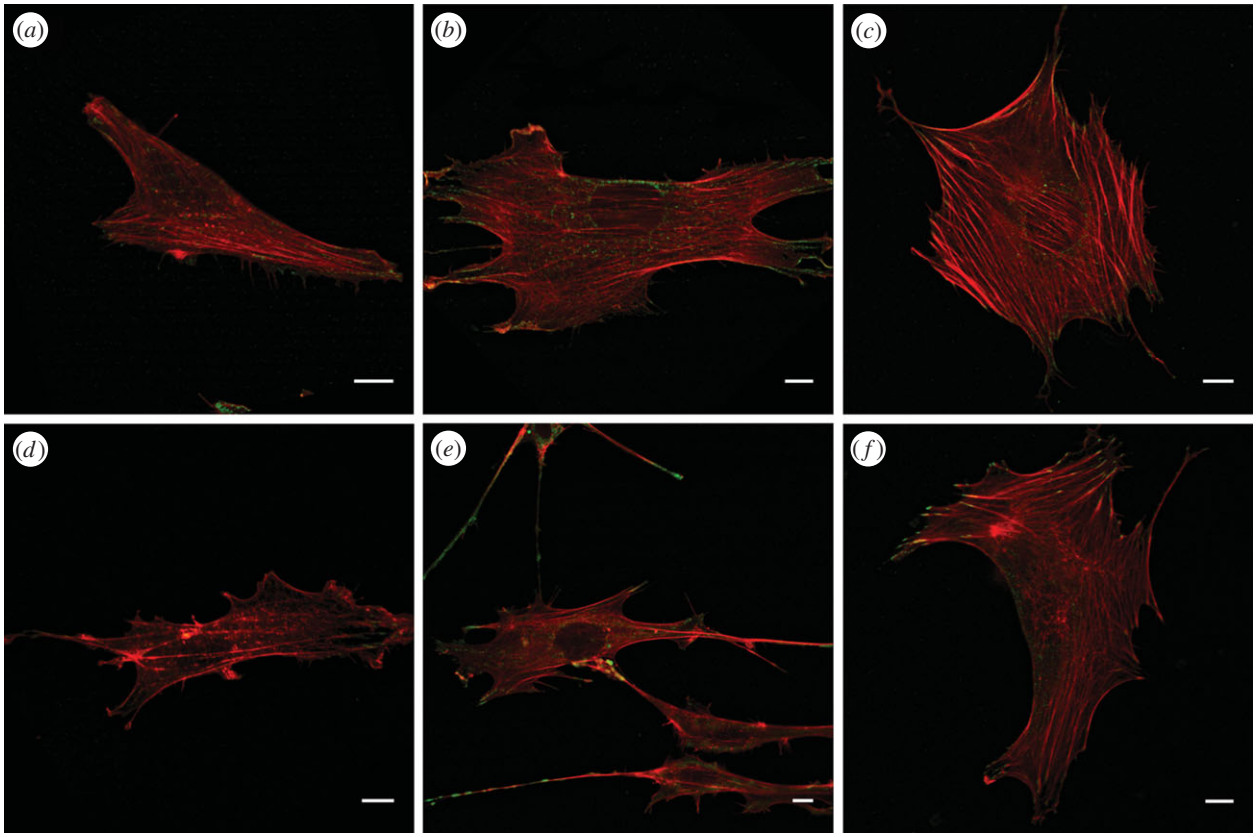

Figure 3. Confocal images of MC3T3 cells cultivated on untreated substrates for 4 h (*a–c*) and 24 h (*d–f*). (*a,d*) Cells on 2 µm pattern; (*b,e*) cells on 5 µm pattern; (*c,f*) cells on flat substrate. Cells were stained for actin fibres (red) and vinculin (green). Scale bars, 10 µm.

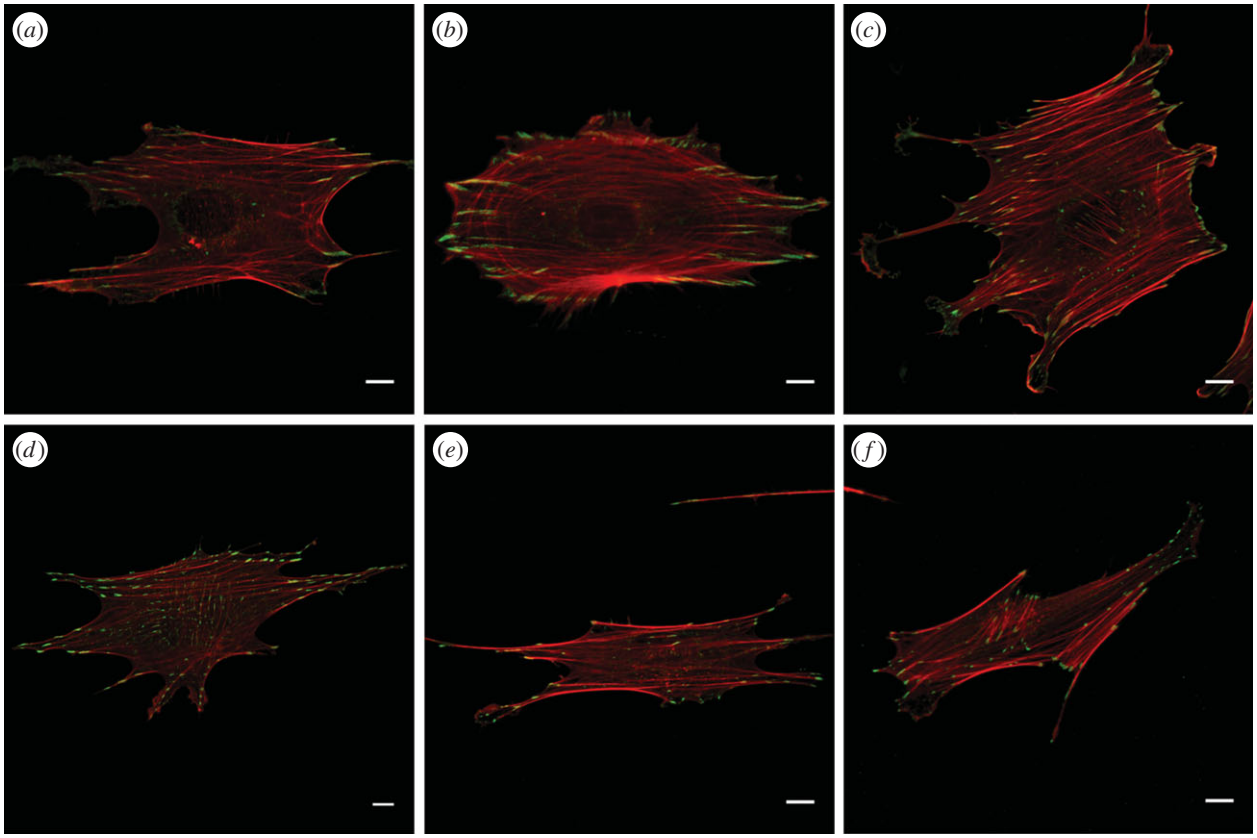

Figure 4. Confocal images of MC3T3 cells cultivated on oxygen PT substrates for 4 h (*a–c*) and 24 h (*d–f*). (*a,d*) Cells on 2 µm pattern; (*b,e*) cells on 5 µm pattern; (*c,f*) cells on flat substrate. Cells were stained for actin fibres (red) and vinculin (green). Scale bars, 10 µm.

FAs and stress fibres were observed on all substrates (figure 4). In particular, the longest FAs were predominantly localized at the top of the ridges, oriented along the pattern direction. On 5 µm patterns, FAs mostly grew on the rough edges of the ridges and small FAs on the grooves were observed occasionally (figure 4*b,e* and electronic supplementary material, figure S5).

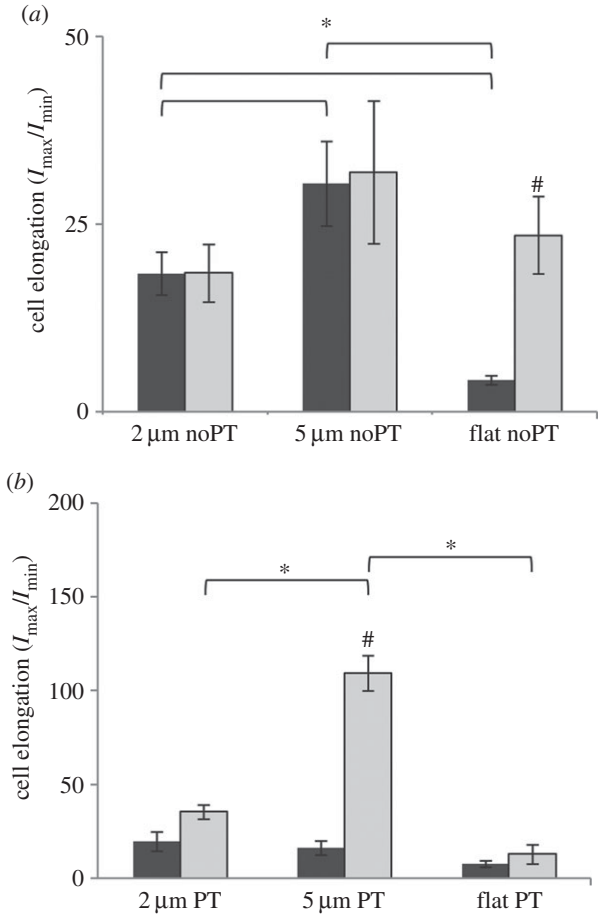

Figure 5. Histograms of the cell elongation index of cells cultivated on untreated substrates (*a*) or oxygen PT substrates (*b*). Dark columns refer to 4 h culturing time; light columns refer to 24 h. Hash (#) indicates a statistically significant difference with respect to the value at 4 h ($p < 0.05$). Asterisk (*) indicates statistically significant differences between groups ($p < 0.05$).

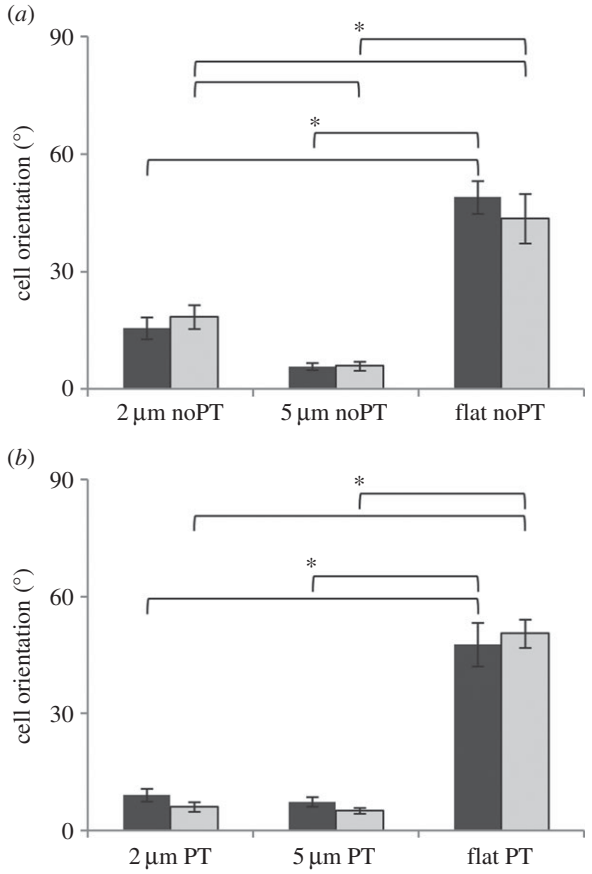

Figure 6. Histograms of the cell orientation with respect to the pattern direction index of cells cultivated on untreated substrates (*a*) or oxygen PT substrates (*b*). Dark columns refer to 4 h culturing time; light columns refer to 24 h. Asterisk (*) indicates statistically significant differences between groups ($p < 0.05$).

Few FAs were also observed in different directions from that of the pattern. These, however, appeared as aligned dots connected by a single actin fibre on 2 µm pattern (figure 4*d*) or as individual FAs on 5 µm pattern (figure 4*b*,*e*).

MC3T3 cells attained an elongated shape within a few hours after seeding, according to the culturing conditions. We investigated how cells perceived the surface features and changed their shape accordingly. Cells on non-treated microtopographies assumed an elongated shape already at 4 h post seeding. Conversely, elongation of cells on flat surfaces occurred at longer times (figure 5*a*). Therefore, topographic signals provided an immediate directional cue for the elongation to occur. Surface plasma treatment affected both the magnitude and the dynamics of cell elongation. In fact, elongation was enhanced when cells were seeded on oxygen PT micropatterns. However, highly elongated cells were observed at long culture times, whereas at 4 h cells were well spread on the surface but displayed a rounder morphology (figure 5*b*). Conversely, cells on flat substrates exhibited a less elongated shape.

Elongation alone does not convey any information on the orientation of cells with respect to the topographic pattern. Therefore, we calculated the orientation of the cell major axis (i.e. principal axis of the moment of area) with respect to the pattern direction, for all the experimental set-ups (figure 6). On untreated surfaces, we observed a strong cell–pattern coalignment in the case of cells seeded on the 5 µm topography at 4 h post seeding. As expected, cells on flat surfaces were randomly oriented. Interestingly, cells on 2 µm patterns displayed an average orientation that was intermediate between the 5 µm topography and the flat case (figure 6*a*). No significant changes in orientation were observed at longer times. Cells on treated surfaces displayed a similar behaviour, except for the 2 µm PT set-up, where a strong cell–pattern coalignment was observed both at 4 and 24 h (figure 6*b*).

3.3. Filopodia and focal adhesions features

Cell spreading and elongation result from filopodial probing and FA establishment and growth. Therefore, we wanted to establish how material surface features interfere with these processes and with cell orientation, consequently. Filopodia were either straight or bent to follow the pattern contour. We observed that the average filopodial length remained unchanged with both topography surface properties, with the only exception of the 5 µm PT case in which filopodia were shorter than the flat PT experiment ($p = 0.003$). However, the distribution of lengths did not exceed 8 µm (electronic supplementary material, figure S6) and the majority of the observed filopodia had a length below 5 µm (figure 7*d*,*e*). This suggests that filopodial probing might be independent from micrometre scale topography and adhesiveness. Conversely, FA length and spatial distribution

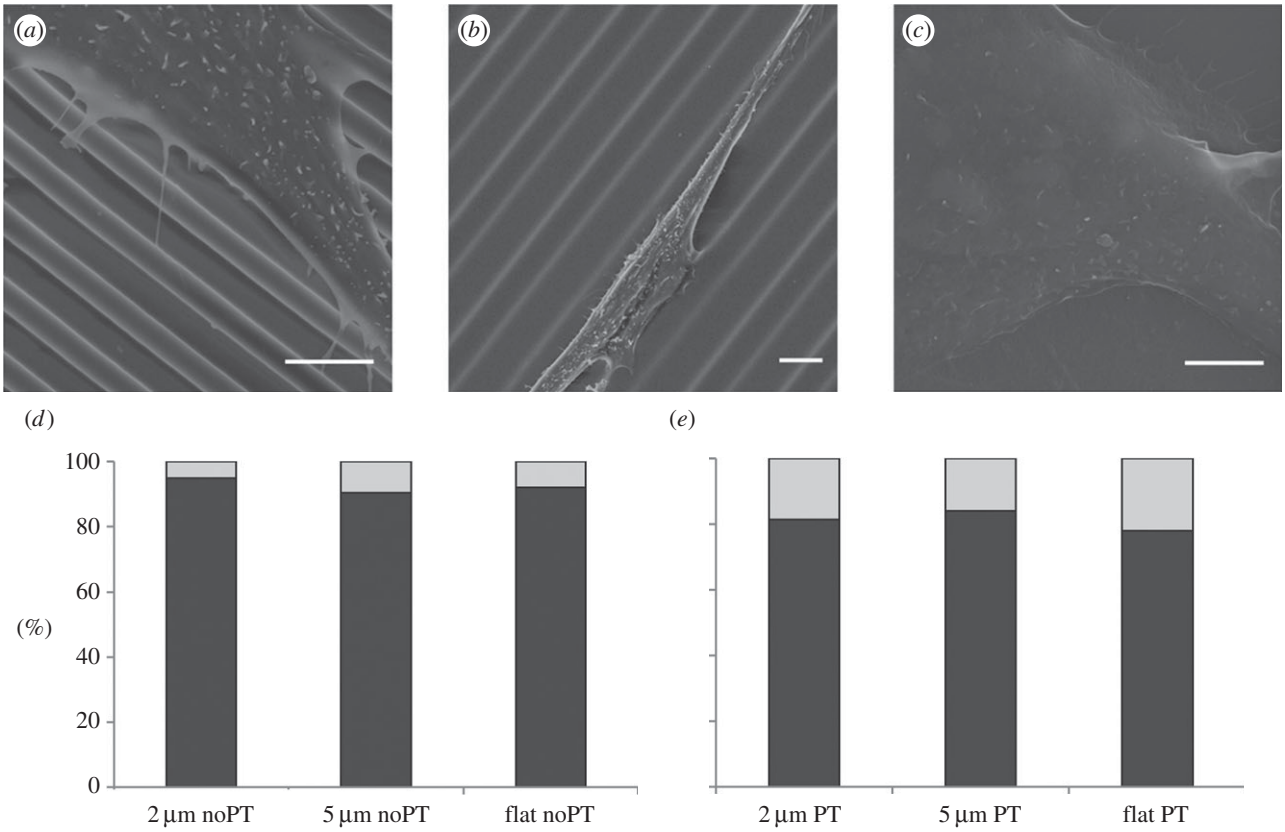

Figure 7. Representative images of filopodia on 2 µm PT (*a*), 5 µm PT (*b*) and flat PT (*c*) substrates. Scale bars, 5 µm. Stacked histograms reporting the percentage fraction of short (less than 5 µm, black columns) and long (more than 5 µm, grey columns) filopodia on untreated (*d*) and oxygen PT substrates (*e*).

changed dramatically. On untreated surfaces and after 4 h of culture, MC3T3 displayed thin and short FAs most of which were not clearly detectable owing to the low contrast produced by the background fluorescence due to the abundant cytoplasmic vinculin. More defined FAs were observed only on flat surfaces at 4 h of culture. At longer culturing times, however, FAs were detectable on all substrates. In particular, the FA signal/cytoplasmic background ratio was sufficiently high to allow us to perform a thorough morphometric characterization. Therefore, we limited our attention to the 24 h culture experiments. In these cases, we were able not only to determine the distribution of FA lengths, but also the orientation relative to the pattern direction (figure 8*a–c*). On oxygen PT substrates, FAs were clearly visible already at 4 h on all the substrate types. However, in order to compare the effects of increased adhesiveness and topography on adhesion assembly, we here present the morphometric analysis at 24 h only (figure 8*d–f*). On pristine or PT substrates, we found that longer FAs were oriented along the pattern direction (0° in figure 8). Fewer and smaller FAs were observed across the pattern direction. As expected, no preferential directions of FA growth were observed on flat substrates. We therefore hypothesized that the FAs, during their maturation, were able to grow in length as much as they could, up to a threshold level that was a function of the orientation. In particular, we assumed the threshold length along the pattern direction to be the maximum length of FAs that we observed on flat substrates (6.6 µm on pristine PDMS or 13.6 µm on PT PDMS, figure 8*c*,*f*). However, if a FA grew across the pattern direction, the width of the topographic feature was assumed to be the threshold length. A further assumption was that FA threshold length varied with the orientation with respect to the pattern direction as the radius of an ellipse. In symbols

$$r = \frac{W \cdot L_{\max}}{\sqrt{L_{\max}^2 - (L_{\max}^2 - W^2)\cos^2\vartheta}}, \tag{3.1}$$

in which W is the minor semiaxis and is equal to the ridge width, $L_{\max}$ is the major semiaxis and is the maximum length that FAs can attain in longitudinal direction, i.e. the maximum length observed on a flat substrate.

According to the morphometric analysis reported in figure 8, our assumptions are valid in the case of 2 µm patterns, both treated and untreated, as most of the FAs were smaller than the threshold value (figure 8*a*,*d*). Conversely, on 5 µm pattern, FAs perpendicular to the pattern direction were smaller than the maximum length available, attaining a value of approximately 2.5 µm (figure 8*b*,*e*).

3.4. Cell migration

Owing to the observed differences in FA maturation and spatial distribution, along with the differences in cell elongation and orientation, we expected that the combined effect of topography and oxygen plasma treatment might be a potent regulator of cell migration. Indeed, cells on untreated 2 µm patterns were able to move extensively across the pattern direction (figure 9*a*). Interestingly, this behaviour changed dramatically when the same pattern was treated with oxygen plasma, in which case cells migrated extensively along the pattern direction (figure 9*d*). Conversely, a strong trajectory–pattern coalignment was observed in the case of cells on 5 µm patterns, both for untreated and treated surfaces (figure 9*b*,*e*). Such a coalignment was amplified on PT substrates. As expected, trajectories of cells

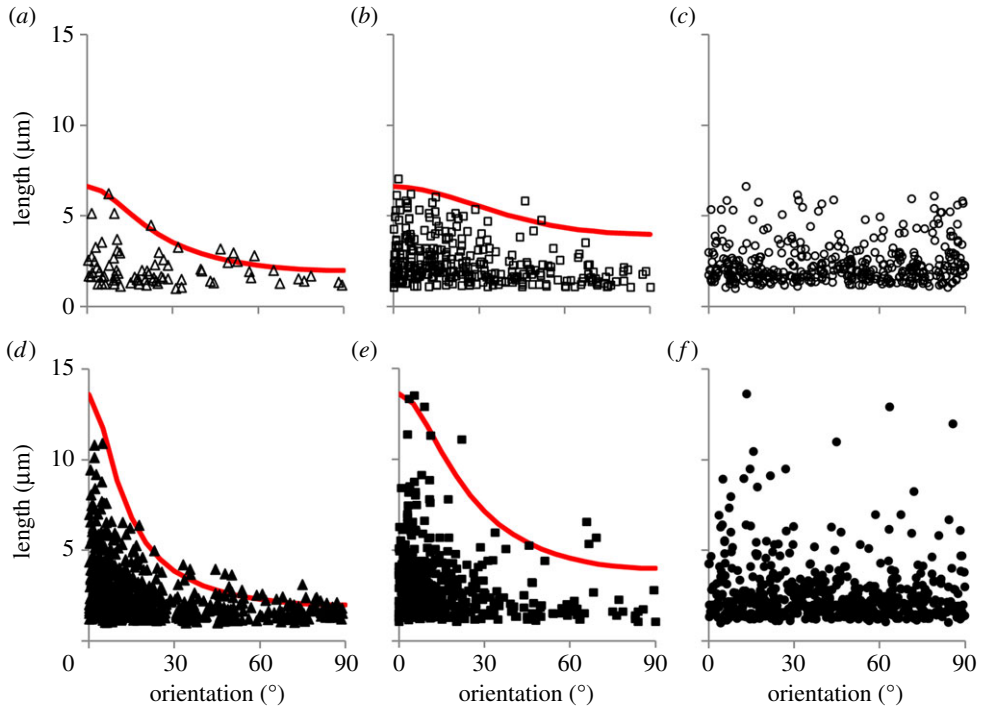

Figure 8. Distribution of FA lengths with respect to pattern orientation. FA measured on untreated substrates (*a*–*c*) and on oxygen PT substrates (*d*–*f*). Two-micrometre pattern (*a*,*d*); 5 μm pattern (*b*,*e*); flat substrates (*c*,*f*). Pattern direction coincides with 0°. For flat substrates, the calculation was performed with respect to the horizontal axis. Solid line describes equation (3.1). (Online version in colour.)

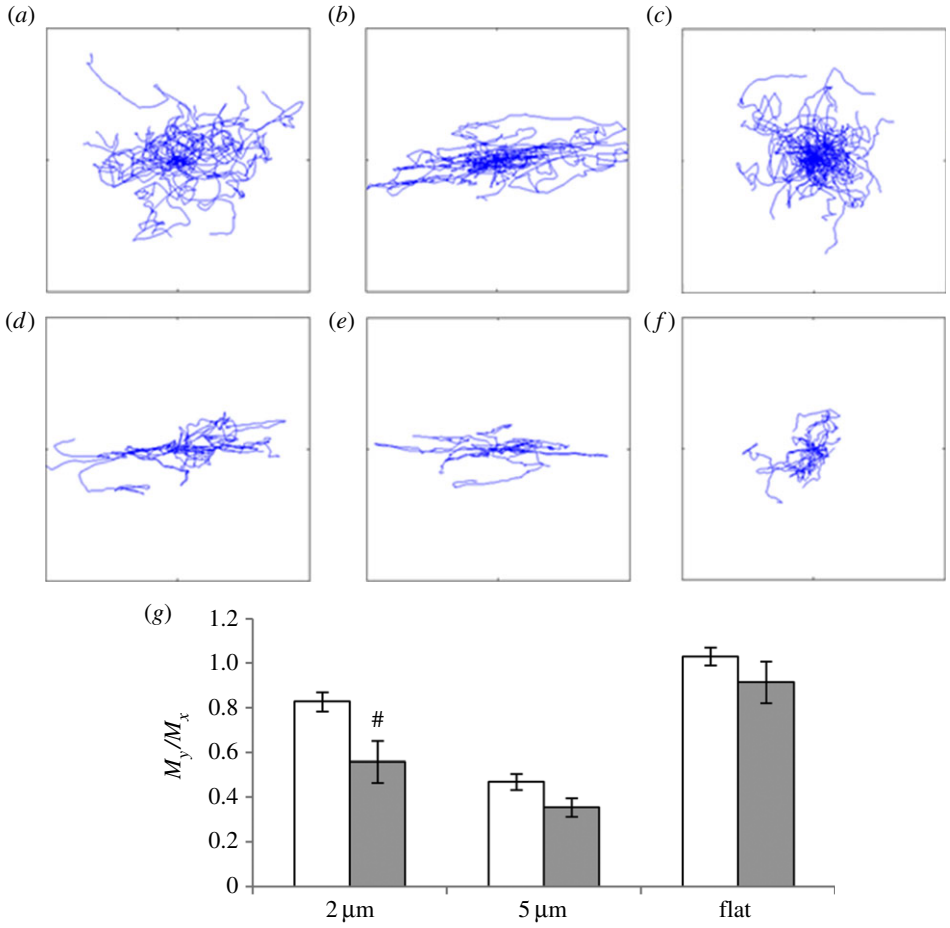

Figure 9. Windrose plots of the trajectories described by cells in 18 h on untreated substrates (*a*–*c*) or oxygen PT substrates (*d*–*f*). Two-micrometre pattern (*a*,*d*); 5 μm pattern (*b*,*e*); flat substrates (*c*,*f*). Plot dimensions are 1000 × 1000 μm. Pattern direction coincides with the horizontal axis. (*g*) Histograms of the directional index. White bars represent cells on untreated substrates. Grey bars represent cells on PT substrates. Error bars are s.e.m. Hash (#) represents significant differences with respect to the noPT case ($p < 0.05$). (Online version in colour.)

migrating on flat substrates were distributed isotropically on the plane (figure 9*c*,*f*).

Accordingly, the quantitative analysis of alignment of cell migration through the evaluation of the directional index revealed a high trajectory pattern coalignment in the case of 5 μm patterns, whereas only the tracks of cells on PT 2 μm patterns exhibited a considerable alignment with the pattern direction (figure 9*g*).

4. Discussion

Adequate integration and cellular colonization of biomaterials are key issues to consider in order to improve functionality and long-term stability of implants. To date, various strategies exploiting different arrays of stimuli have been pursued in order to guide cells to the implant site and controlling their behaviour therein. However, the optimal set of stimuli able to elicit the desired cell response has not been identified yet. Topography is a potent signal that has proved to be very effective in regulating cell adhesion, proliferation and migration. Furthermore, topographic patterns can be embossed on artificial surfaces with great accuracy and over large areas. Owing to these advantages, several types of devices presenting patterned surfaces were fabricated and tested for various applications. For example, Curtis *et al.* [23] proposed a micropatterned PDMS sheath for *in situ* tendon repair that effectively guided collagen biosynthesis and assembly with normal histology. More recently, Rani *et al.* [24] have reported improved *in vivo* osteointegration of nanopatterned titanium implants. Altogether, these data demonstrate the effectiveness of topography in *in vivo* settings, where the spatial and temporal stability of the presented signals is key. Yet, the best way to present topographies able to elicit the desired cell functions has not been defined. This becomes particularly relevant in the case of surfaces able to affect cell morphology, orientation and migration. These aspects are crucial when it is desired to replicate the supracellular patterns observed *in vivo*. However, a fully effective topography mediated cell control, both *in vivo* and *in vitro*, has not been achieved yet, owing to our modest understanding of the basic principles that regulate cell–topography interactions. In order to gain a better understanding of the way cells perceive and react to topographies, we used microgrooved substrates whose features had characteristic lengths that interfere with cell filopodial probing and FA establishment and growth. The probing mechanism is strongly connected to filopodia length. Literature data report an average length of filopodia of the order of 1–5 μm [15,25,26]. We confirmed that this dimension is still valid in the case of micropatterned surfaces. In particular, we found that filopodia length rarely surpassed 5 μm (figure 7*d*,*e*). Adhesion formation is subsequent to filopodial probing. Once formed, adhesions grow in length; this process may be hindered by the presence of topographic patterns [4]. Preliminary experiments performed on flat surfaces provided us with information on the average FA length that MC3T3 cells are able to assemble on PDMS substrates (2.39 ± 1.12 μm). Furthermore, we noted that the hydrophobic/hydrophilic characteristics of the surface alter FA maturation. In fact, as reported by Llopis-Hernández *et al.* [27], FA formation is enhanced on more hydrophilic surfaces, because there is an increased availability of binding domains of the physisorbed protein layer. Indeed, we found that on oxygen PT surfaces

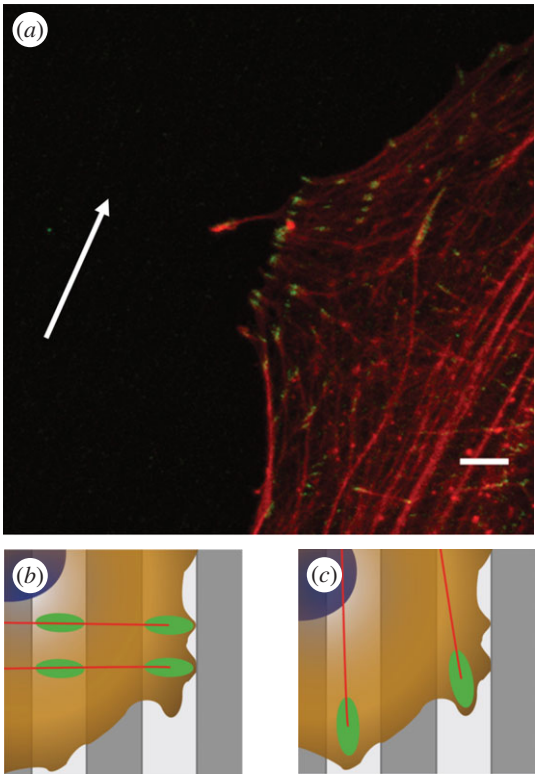

Figure 10. (*a*) Detail of FAs of MC3T3 cultivated on oxygen plasma-treated 2 μm pattern. Vinculin labelled with Alexa Fluor 488 in green. Actin bundles are stained with TRITC-phalloidin in red. Pattern is oriented as the white arrow. Scale bar, 5 μm. (*a*,*b*) Schematic of FA growth on oxygen PT substrates. FAs can grow considerably and their lengths surpass ridge dimension. In this case, FAs are observed in a dashed and unstable conformation (*b*), favouring cell elongation along the pattern direction (*c*).

FAs are longer and wider and can reach a length of up to 13 μm (figure 8*f*). Additionally, topographic patterns are known to alter surface wettability and to adsorb serum proteins non-uniformly [28], but the total mass of adsorbed proteins does not change with respect to flat surfaces [28]. Therefore, differences in terms of adhesion and migration have to be ascribed to the local ligand presentation, which in turn is modulated by topography and chemical surface characteristics.

FAs were mostly observed on the top of the ridges of the 2 and 5 μm patterns. In the latter case, however, a very limited number of FAs were also on the grooves both at 4 and 24 h. Filopodia have sufficient mobility and length to come in contact with the deep topographic recesses. In principle, these filopodia can establish new focal contacts, but apparently this event is unfavoured in contrast to FA formation on the ridges. In fact, as demonstrated by Albuschies & Vogel [29], FA formation is impaired when the angle between the filopodia and the adhesion plane is high (12° on glass). Such an impairment is caused by high normal stresses acting on the FA, which are responsible for integrin–ligand complex disruption. An analogous circumstance may occur when filopodia penetrate into the recesses of the topographic patterns. In our patterns, filopodia may form non-zero angles with the adhesion plane. Five-micrometre pattern seemed to be a more permissive configuration for FAs to establish on the groove top, owing to the smaller aspect ratio of the topographic feature. Therefore, topographic patterns create preferential zones for the adhesion plaques to establish and grow. The cell traction machinery constituted by actin stress fibres, which are responsible for cell polarization and

migration, is also affected by the geometrical features of the adhesion plaques and, hence, by the spatial distribution of adsorbed proteins. Ultimately, ordered topographic patterns, in the form of gratings and grooves, produce pathways for the cell adhesion plaques, thus altering spreading and cell migration [30,31]. In particular, cells on 5 μm patterns displayed a high elongation and strong coalignment with the pattern direction. This is reflected in the direction of migration, which was remarkably close to the pattern direction. Cells on 2 μm patterns had a bimodal behaviour, i.e. their behaviour in terms of coalignment, elongation and migration was intermediate between that observed for cells on untreated 5 μm pattern and flat substrates. Conversely, they behaved in a more similar way to 5 μm pattern when the substrate was subjected to oxygen plasma treatment. Accordingly, we found long FAs directed along the pattern in the case of cells exhibiting a strong coalignment with the pattern. However, a considerable fraction of FAs directed perpendicularly was found for both the plasma-treated 5 and 2 μm patterns. In the first case, FAs were isolated and did not occupy the whole pattern ridge or groove (figure 8*e*). Actin fibres connected to these FAs resembled uncontractile dorsal stress fibres [32], whereas longitudinal FAs were anchored to thicker and contractile ventral stress fibres. Therefore, on 5 μm patterns, the establishment of transverse adhesions is admissible, but their maturation is unfavoured with respect to FAs growing along the pattern. On plasma-treated 2 μm patterns, we observed transverse adhesions in the form of dashed structures. Interestingly, these adhesions were connected by isolated actin bundles, suggesting that dashed adhesions might indeed belong to the same entity (figure 10*a*). According to Balaban *et al*. [33], actin-generated forces regulate FA area in order to maintain shear stress at the adhesion site at the constant value (5.5 nN μm^{-2}). If FA growth cannot keep up with increasing tensile forces, being geometrically confined, the resistance in the transverse direction is reduced, owing to a less extended contact area (figure 10*b*). Therefore, adhesion sites in the transverse direction have a higher probability of disassembling, whereas longer and mature adhesions that elongate along the ridges are more stable (figure 10*c*). This results in elongation of cells along the pattern direction with an increased directional migration.

5. Conclusion

This work investigates the combinatorial effects of micrometre scale topography and chemical characteristics of the surface on the adhesion and migratory behaviour of MC3T3 cells. Our results suggest the existence of two characteristic lengths of the topographic features, according to which cells may react differently. In the context of topographies with long-range order and specifically microgratings, cells are not able to perceive ridges that are placed farther than the length of filopodia, whose dimension span in the 1–6 μm range. Also, when ridges reach dimensions capable of interfering with FA maturation, strong effects on cell elongation and migration are observed. In particular, FA growth is intimately connected to ligands' availability and conformation, which in turn are strongly affected by the chemical properties of the surface. Thus, different chemical surface properties induce different FA dynamics and therefore alter the way cells perceive the topography. This suggests that topography might not be a signal *per se*, but the way it is perceived is strongly mediated by proteins absorbed on the surface and hence by the spatial positioning of ligands. Therefore, we would expect very similar results in the case of biochemical patterns constituted by micrometric stripes of adhesive proteins, separated by antiadhesive regions. This does not necessarily mean that topographic signals can always be substituted by biochemical patterns. In fact, topographic signals are easier to encode on synthetic surfaces, can be reproduced with a high consistency and are very stable under harsh processing conditions and also in *in vivo* settings.

Acknowledgements. The authors thank Ms V. La Tilla for drawings and figure formatting, Mrs R. Infranca for the manuscript proofreading and Dr M. Colella for the SEM examinations.

References

1. Last JA, Liliensiek SJ, Nealey PF, Murphy CJ. 2009 Determining the mechanical properties of human corneal basement membranes with atomic force microscopy. *J. Struct. Biol.* **167**, 19–24. (doi:10.1016/j.jsb.2009.03.012)
2. Liliensiek SJ, Nealey P, Murphy CJ. 2009 Characterization of endothelial basement membrane nanotopography in rhesus macaque as a guide for vessel tissue engineering. *Tissue Eng. A* **15**, 2643–2651. (doi:10.1089/ten.tea.2008.0284)
3. Gutsmann T, Fantner GE, Kindt JH, Venturoni M, Danielsen S, Hansma PK. 2004 Force spectroscopy of collagen fibers to investigate their mechanical properties and structural organization. *Biophys. J.* **86**, 3186–3193. (doi:10.1016/S0006-3495(04)74366-0)
4. Natale CF, Ventre M, Netti PA. 2014 Tuning the material-cytoskeleton crosstalk via nanoconfinement of focal adhesions. *Biomaterials* **35**, 2743–2751. (doi:10.1016/j.biomaterials.2013.12.023)
5. Vandrovcova M, Hanus J, Drabik M, Kylian O, Biederman H, Lisa V, Bacakova L. 2012 Effect of different surface nanoroughness of titanium dioxide films on the growth of human osteoblast-like MG63 cells. *J. Biomed. Mater. Res. A* **100**, 1016–1032. (doi:10.1002/jbm.a.34047)
6. Lamers E, van Horssen R, te Riet J, van Delft FC, Luttge R, Walboomers XF, Bacakova L. 2010 The influence of nanoscale topographical cues on initial osteoblast morphology and migration. *Eur. Cells Mater.* **20**, 329–343.
7. Yim EK, Pang SW, Leong KW. 2007 Synthetic nanostructures inducing differentiation of human mesenchymal stem cells into neuronal lineage. *Exp. Cell Res.* **313**, 1820–1829. (doi:10.1016/j.yexcr.2007.02.031)
8. Dalby MJ, Gadegaard N, Tare R, Andar A, Riehle MO, Herzyk P, Wilkinson CD, Oreffo RO. 2007 The control of human mesenchymal cell differentiation using nanoscale symmetry and disorder. *Nat. Mater.* **6**, 997–1003. (doi:10.1038/nmat2013)
9. Ventre M, Causa F, Netti PA. 2012 Determinants of cell–material crosstalk at the interface: towards engineering of cell instructive materials. *J. R. Soc. Interface* **9**, 2017–2032. (doi:10.1098/rsif.2012.0308)
10. Yang Y, Leong KW. 2010 Nanoscale surfacing for regenerative medicine. *Wiley Interdiscip. Rev. Nanomed. Nanobiotechnol.* **2**, 478–495. (doi:10.1002/wnan.74)
11. Kim HN, Kang DH, Kim MS, Jiao A, Kim DH, Suh KY. 2012 Patterning methods for polymers in cell and tissue engineering. *Ann. Biomed. Eng.* **40**, 1339–1355. (doi:10.1007/s10439-012-0510-y)
12. Pot SA, Liliensiek SJ, Myrna KE, Bentley E, Jester JV, Nealey PF, Murphy CJ. 2010 Nanoscale topography-induced modulation of fundamental cell behaviors of rabbit corneal keratocytes, fibroblasts, and myofibroblasts. *Invest. Ophthalmol. Vis. Sci.* **51**, 1373–1381. (doi:10.1167/iovs.09-4074)

13. Loesberg WA, te Riet J, van Delft FC, Schön P, Figdor CG, Speller S, van Loon JJ, Walboomers XF, Jansen JA. 2007 The threshold at which substrate nanogroove dimensions may influence fibroblast alignment and adhesion. *Biomaterials* **28**, 3944–3951. (doi:10.1016/j.biomaterials.2007.05.030)
14. Mattila PK, Lappalainen P. 2008 Filopodia: molecular architecture and cellular functions. *Nat. Rev. Mol. Cell Biol.* **9**, 446–454. (doi:10.1038/nrm2406)
15. Schäfer C, Faust U, Kirchgessner N, Merkel R, Hoffmann B. 2011 The filopodium: a stable structure with highly regulated repetitive cycles of elongation and persistence depending on the actin cross-linker fascin. *Cell Adhes. Migr.* **5**, 431–438. (doi:10.4161/cam.5.5.17400)
16. Parsons JT, Horwitz AR, Schwartz MA. 2010 Cell adhesion: integrating cytoskeletal dynamics and cellular tension. *Nat. Rev. Mol. Cell Biol.* **11**, 633–643. (doi:10.1038/nrm2957)
17. Biggs MJ, Richards RG, McFarlane S, Wilkinson CD, Oreffo RO, Dalby MJ. 2008 Adhesion formation of primary human osteoblasts and the functional response of mesenchymal stem cells to 330 nm deep microgrooves. *J. R. Soc. Interface* **5**, 1231–1242. (doi:10.1098/rsif.2008.0035)
18. Keselowsky BG, Collard DM, García AJ. 2003 Surface chemistry modulates fibronectin conformation and directs integrin binding and specificity to control cell adhesion. *J. Biomed. Mater. Res. A* **66**, 247–259. (doi:10.1002/jbm.a.10537)
19. Seo CH, Jeong H, Furukawa KS, Suzuki Y, Ushida T. 2013 The switching of focal adhesion maturation sites and actin filament activation for MSCs by topography of well-defined micropatterned surfaces. *Biomaterials* **34**, 1764–1771. (doi:10.1016/j.biomaterials.2012.11.031)
20. Maruoka M, Sato M, Yuan Y, Ichiba M, Fujii R, Ogawa T, Ishida-Kitagawa N, Takeya T, Watanabe N. 2012 Abl-1-bridged tyrosine phosphorylation of VASP by Abelson kinase impairs association of VASP to focal adhesions and regulates leukaemic cell adhesion. *Biochem. J.* **441**, 889–899. (doi:10.1042/BJ20110951)
21. Biela SA, Su Y, Spatz JP, Kemkemer R. 2009 Different sensitivity of human endothelial cells, smooth muscle cells and fibroblasts to topography in the nano-micro range. *Acta Biomater.* **5**, 2460–2466. (doi:10.1016/j.actbio.2009.04.003)
22. Murakami D, Jinnai H, Takahara A. 2014 Wetting transition from the Cassie–Baxter state to the Wenzel state on textured polymer surfaces. *Langmuir* **30**, 2061–2067. (doi:10.1021/la4049067)
23. Curtis AS, Wilkinson CD, Crossan J, Broadley C, Darmani H, Johal KK, Jorgensen H, Monaghan W. 2005 An *in vivo* microfabricated scaffold for tendon repair. *Eur. Cells Mater.* **9**, 50–57.
24. Rani VV, Vinoth-Kumar L, Anitha VC, Manzoor K, Deepthy M, Shantikumar VN. 2012 Osteointegration of titanium implant is sensitive to specific nanostructure morphology. *Acta Biomater.* **8**, 1976–1989. (doi:10.1016/j.actbio.2012.01.021)
25. Mogilner A, Rubinstein B. 2005 The physics of filopodial protrusion. *Biophys. J.* **89**, 782–795. (doi:10.1529/biophysj.104.056515)
26. Husainy AN, Morrow AA, Perkins TJ, Lee JM. 2010 Robust patterns in the stochastic organization of filopodia. *BMC Cell Biol.* **11**, 86. (doi:10.1186/1471-2121-11-86)
27. Llopis-Hernández V, Rico P, Ballester-Beltrán J, Moratal D, Salmerón-Sánchez M. 2011 Role of surface chemistry in protein remodeling at the cell-material interface. *PLoS ONE* **6**, e19610. (doi:10.1371/journal.pone.0019610)
28. Papenburg BJ, Rodrigues ED, Wessling M, Stamatialis D. 2010 Insights into the role of material surface topography and wettability on cell-material interactions. *Soft Matter* **6**, 4377–4388. (doi:10.1039/B927207K)
29. Albuschies J, Vogel V. 2013 The role of filopodia in the recognition of nanotopographies. *Sci. Rep.* **3**, 1658. (doi:10.1038/srep01658)
30. von Recum AF, van Kooten TG. 1995 The influence of micro-topography on cellular response and the implications for silicone implants. *J. Biomater. Sci. Polym. Ed.* **7**, 181–198. (doi:10.1163/156856295X00698)
31. den Braber ET, de Ruijter JE, Ginsel LA, von Recum AF, Jansen JA. 1998 Orientation of ECM protein deposition, fibroblast cytoskeleton, and attachment complex components on silicone microgrooved surfaces. *J. Biomed. Mater. Res.* **40**, 291–300. (doi:10.1002/(SICI)1097-4636(199805)40:2<291::AID-JBM14>3.0.CO;2-P)
32. Tojkander S, Gateva G, Schevzov G, Hotulainen P, Naumanen P, Martin C, Gunning PW, Lappalainen P. 2011 A molecular pathway for myosin II recruitment to stress fibers. *Curr. Biol.* **21**, 539–550. (doi:10.1016/j.cub.2011.03.007)
33. Balaban NQ *et al.* 2001 Force and focal adhesion assembly: a close relationship studied using elastic micropatterned substrates. *Nat. Cell Biol.* **3**, 466–472. (doi:10.1038/35074532)